Characterization and validation of noninvasive oxygen tension measurements in human glioma xenografts by 19F-MR relaxometry

Boudewijn P. J. van der Sanden, Arend Heerschap, Arjan W. Simonetti, Paul F. J. W. Rijken, Hans P. W. Peters, Georg Stüben, Albert J. van der Kogel

Angaben zur Veröffentlichung / Publication details:

Sanden, Boudewijn P. J. van der, Arend Heerschap, Arjan W. Simonetti, Paul F. J. W. Rijken, Hans P. W. Peters, Georg Stüben, and Albert J. van der Kogel. 1999. "Characterization and validation of noninvasive oxygen tension measurements in human glioma xenografts by 19F-MR relaxometry." *International Journal of Radiation Oncology*Biology*Physics* 44 (3): 649–58. https://doi.org/10.1016/s0360-3016(98)00555-0.

CHARACTERIZATION AND VALIDATION OF NONINVASIVE OXYGEN TENSION MEASUREMENTS IN HUMAN GLIOMA XENOGRAFTS BY ^{19}F-MR RELAXOMETRY

BOUDEWIJN P. J. VAN DER SANDEN, M.Sc.,* AREND HEERSCHAP, Ph.D.,* ARJAN W. SIMONETTI, M.Sc.,* PAUL F. J. W. RIJKEN, M.Sc.,† HANS P. W. PETERS,† GEORG STÜBEN, M.D.,‡ AND ALBERT J. VAN DER KOGEL, Ph.D.†

Departments of *Radiology and †Radiotherapy, University Hospital, Nijmegen, The Netherlands; and ‡Department of Radiotherapy, University Hospital, Essen, Germany

Purpose: The aim of this study was to characterize and to validate noninvasive ^{19}F-magnetic resonance relaxometry for the measurement of oxygen tensions in human glioma xenografts in nude mice. The following three questions were addressed: 1. When perfluorocarbon compounds (PFCs) are administrated intravenously, which tumor regions are assessed by ^{19}F-MR relaxometry? 2. Are oxygen tension as detected by ^{19}F-MR relaxometry ($pO_{2/relaxo}$) comparable to Eppendorf O_2-electrode measurements ($pO_{2/electrode}$)? 3. Can ^{19}F-MR relaxometry be used to detect oxygen tension changes in tumor tissue during carbogen breathing?

Methods and Materials: Slice-selective ^{19}F-MR relaxometry was carried out with perfluoro-15-crown-5-ether as oxygen sensor. The PFC was injected i.v. 3 days before the ^{19}F-MR experiments. Two datasets were acquired before and two after the start of carbogen breathing. The distribution of PFCs and necrotic areas were analyzed in ^{19}F-Spin Echo (SE) density MR images and T_2-weighted ^{1}H-SE MR images, respectively. One day after the MR investigations, oxygen tensions were measured by oxygen electrodes in the same slice along two perpendicular tracks. These measurements were followed by (immuno)histochemical analysis of the 2D distribution of perfused microvessels, hypoxic cells, necrotic areas, and macrophages.

Results: The PFCs mainly became sequestered in perfused regions at the tumor periphery; thus, ^{19}F-MR relaxometry probed mean oxygen tensions in these regions throughout the selected MR slice. In perfused regions of the tumor, mean $pO_{2/relaxo}$ values were comparable to mean $pO_{2/electrode}$ values, and varied from 0.03 to 9 mmHg. Median $pO_{2/electrode}$ values of both tracks were lower than mean $pO_{2/relaxo}$ values, because low $pO_{2/electrode}$ values that originate from hypoxic and necrotic areas were also included in calculations of median $pO_{2/electrode}$ values. After 8-min carbogen breathing, the average $pO_{2/relaxo}$ increase was 3.3 ± 0.8 (SEM) mmHg and 2.1 ± 0.6 (SEM) after 14 min breathing.

Conclusions: We have demonstrated that PFCs mainly became sequestered in perfused regions of the tumor. Here, mean $pO_{2/relaxo}$ values were comparable to mean $pO_{2/electrode}$ values. In these areas, carbogen breathing was found to increase the $pO_{2/relaxo}$ values significantly.

^{19}F-MR relaxometry, Polarography, Gliomas, Oxygen tension, Carbogen.

INTRODUCTION

It has been shown that the oxygen tension of tumor tissue is an important physiological parameter during radiotherapy treatment (1–3). Hypoxic tumor cells are approximately 3 times more radioresistant than well-oxygenated cells (1). Therefore, modulations of the oxygen tension in tumor tissue may enhance the sensitivity of tumor cells for radiotherapy. For example, breathing of carbogen (95% O_2, 5% CO_2) has been introduced to decrease the fraction of chronically hypoxic cells (4–6). The combination of carbogen breathing with the administration of nicotinamide has produced a significant increase in local control of advanced laryngeal tumors (7).

A method to assess local or global oxygen tensions in tumor tissue would be valuable and may be used to predict the outcome of a treatment modality. Polarography (Eppen-

Presented in part at the 4th Annual Meeting of the International Society for Magnetic Resonance in Medicine, New York, April 1996 and the 14th Annual Meeting of the European Society for Magnetic Resonance in Medicine and Biology, Brussels, September 1997.

Reprint requests to: Dr. Boudewijn P. J. van der Sanden, Department of Radiology, University Hospital Nijmegen, P. O. Box 9101, 6500 HB, Nijmegen, The Netherlands.

Acknowledgements—The authors thank E. van den Boogert and D. Klomp for technical assistance, A. Hansen and colleagues of the Central Animal Laboratory for animal care and Dr. R.J. Hodgkiss of the CRC Gray Laboratory, Mount Vernon Hospital, Northwood, Middlesex, UK for the generous gift of the hypoxic marker NITP. The ^{19}F-MR relaxometry measurements were carried out in collaboration with the Dutch HF-NMR facilities at the Biophysical Chemistry Department of Professor Dr. C.W. Hilbers at the Nijmegen University. This study was supported by the Dutch Cancer Society and, in part, by the "Maurits and Anna de Kock" Foundation.

Accepted for publication 11 December 1998.

dorf O_2 electrodes) is the most frequently used technique for direct measurements of local or global oxygen tensions in tumor tissue ($pO_{2/electrode}$) (8, 9). Although oxygen electrodes are small, polarographic measurements are invasive and studies of deep tumors are difficult or even impossible without surgery.

^{19}F-magnetic resonance relaxometry (^{19}F-MR relaxometry) using perfluorocarbon (PFC) compounds is a noninvasive technique that permits the determination of local or global oxygen tensions in tumors ($pO_{2/relaxo}$), independent of the location of the tumor (10–17). This technique is based on the linear relationship between the spin-lattice relaxation rates ($1/T_1$) of ^{19}F-spins in PFCs and the local oxygen tension in tumor tissue. In most ^{19}F-MR relaxometry studies, PFCs are administered i.v. a few days before the MR measurements (11–15). After approximately 3 days, PFCs had accumulated in tumor tissue and in the reticuloendothelial system of liver and spleen, and PFCs were not detectable in blood plasma (11, 15, 18).

Before ^{19}F-MR relaxometry can be used as an indicator of absolute oxygen tensions or oxygen tension changes in tumor tissue, it will need extensive comparison with more established techniques, such as polarography. A proper comparison between both techniques is possible when the distribution of PFC compounds is spatially correlated to the approximate location of the O_2 electrodes. In addition, it is necessary to know how the distribution of the PFCs and the location of the O_2-electrode tracks are spatially correlated to the distribution of perfused, hypoxic, and necrotic tumor areas. The extent of the latter areas determines local or global oxygen tensions in tumors, and can be used to explain possible differences of pO_2 values as probed by both methods. Furthermore, validation of $pO_{2/relaxo}$ values with $pO_{2/electrode}$ values is of interest because $pO_{2/relaxo}$ values are derived from T_1-relaxation rates of ^{19}F-spins in perfluorocarbon compounds and, in principle, these relaxation rates may also depend on other physiological and histological parameters.

The aim of this study was to characterize and to validate *in vivo* ^{19}F-MR relaxometry as a tool to measure oxygen tensions and changes in oxygen tensions noninvasively in human glioma xenografts. The following questions were addressed: When perfluorocarbon compounds (PFCs) are administrated i.v., which tumor regions are assessed by ^{19}F-MR relaxometry? How are the $pO_{2/relaxo}$ values related to $pO_{2/electrode}$ values? Finally, can ^{19}F-MR relaxometry be used to detect oxygen tension changes in tumor tissue during carbogen breathing?

To answer these questions, the 2D distribution of perfluorocarbon compounds in ^{19}F-MR images was compared to the 2D distribution of perfused microvessels, hypoxic regions, macrophages (18), and necrotic areas using histochemical analysis (19) and T_2-weighted ^{1}H-MR images, respectively. In a previous study (18), it had been suggested that PFCs are taken up by macrophages and, therefore, the distribution of the latter was also compared to the PFC distribution. For each tumor, both $pO_{2/relaxo}$ and $pO_{2/electrode}$ values were sampled in comparable slices through the center of tumors and oxygen tensions changes were measured during carbogen breathing.

MATERIALS AND METHODS

Animal model

Human glioma xenografts (line E49) were grown subcutaneously in the hindlimbs of 13 athymic mice (Balb/c nu/nu, BonholdGard, Ry, Denmark) (20). In pilot studies on the feasibility of slice-selective ^{19}F-MR relaxometry, measurements of oxygen tensions in 2 homogeneously perfused human glioma xenograft lines (E98, E106) (20) and a heterogeneously perfused line (E49), the PFC uptake was only sufficient for slice-selective ^{19}F-MR relaxometry measurements in tumor line E49. Tumor volumes (cm^3) of the latter line were estimated from the formula: $(\pi/6) \times abc$, where a, b, and c are orthogonal diameters as measured with calipers. Mice were anesthetized with 2 % enflurane in an oxygen-nitrous (25% O_2) gas mixture applied through a nose cone. For experiments with carbogen breathing, the oxygen-nitrous gas mixture was switched to carbogen (95% O_2/5% CO_2) and the percentage of enflurane was kept constant. The flow velocity was 1 $l.min^{-1}$ in all experiments, and the composition of gas mixtures was analyzed online at the inlet of the nose cone with a gas monitor (Datascope Multinex, Datascope Corp. Paramus, NJ). All experiments were started 5 min after the beginning of carbogen breathing. The 5-min prebreathing time was based on results of near-infrared spectroscopy experiments, which showed that, after 5 min, the oxyhemoglobin concentration was close to a steady state (21). Body temperature was monitored with a rectal probe (36-gauge wire, Hewlett Packard) and maintained at 36.5°–37° C by a warm water blanket with a feedback system. The anesthesia and temperature control were similar for the *in vivo* ^{19}F-MR relaxometry studies and the polarography measurements (see next sections); thus, possible effects of, for example, anesthesia on the results of both experiments were comparable.

The experimental procedures were approved by the local ethical committee for animal use.

^{19}F-MR relaxometry

^{19}F-MR relaxometry measurements were performed on an SMIS spectrometer interfaced to a vertical bore magnet (4.3 T), employing a home-built ^{1}H/^{19}F double tunable solenoid (∅ 13 mm).

In vitro *experiments.* An *in vitro* calibration curve [$1/T_1$ (s^{-1}) vs. pO_2, mmHg] was generated using an inversion-recovery T_1-sequence with a 180° adiabatic full passage inversion pulse (22) and a 90° hard excitation pulse. The PFC emulsion (40% (v/v) perfluoro-15-crown-5-ether, HemaGen/PFC, St. Louis, MO) was bubbled for 60 min with 5 different gas mixtures (O_2/N_2) containing 0%, 10%, 21%, 48%, and 100% O_2. During the T_1 measurements, gas mixtures were led smoothly over the emulsion to maintain

pO_2 levels. The temperature of the emulsion was monitored online and was kept at 37° C using the same feedback system and rectal probe as mentioned in the previous paragraph. For low pO_2 values, the T_1-relaxation time of ^{19}F-spins is relatively long; thus, a different array of delay times between inversion and excitation pulse was used for correct measurements of the different T_1-relaxation times. For the gas mixtures containing 0% and 10% O_2, the 8 delay times of inversion (TIs) varied between 0.2 and 6 s and, for the other gas mixtures, the TIs ranged from 0.2 to 3 s. The *in vitro* calibration curve was determined from 3 independent measurements.

In vivo *experiments.* Three days before the NMR experiments, 0.15 ml of the 40% (v/v) PFC emulsion was injected *via* a tail vein (dose: 4.2 g/kg). For the appropriate positioning of a coronal slice for ^{19}F-MR relaxometry studies through the center of the tumor parallel to the solenoid coil, multislice coronal T_2-weighted ^{1}H-spin echo images (SE images) were acquired (TR = 1 s, TE = 0.06 s, number of scans = 2, matrix size = 128 × 128, FOV 15 × 15 mm, slice thickness 1.5 mm). Simultaneously, these T_2-weighted ^{1}H-SE images were used for analysis of the necrotic area distribution in comparable slices as observed in *in vivo* ^{19}F-MR experiments. The water diffusion coefficient was found to be larger in necrotic areas than in vital tumor areas (23), which may result in higher signal intensities in T_2-weighted ^{1}H-SE images. Next, ^{19}F-SE density images were obtained at the same position as the ^{1}H-SE images using the following parameters: TR = 8 s, TE = 0.03 s, NS = 2, matrix size = 64 × 64, FOV = 15 × 15 mm, and slice thickness 4 mm. The ^{19}F-SE density images were used for analysis of the 2D distribution of PFCs in similar slices as used in *in vivo* ^{19}F-MR relaxometry studies.

In vivo ^{19}F-MR relaxometry studies were performed with a slice-selective inversion-recovery T_1 sequence with similar acquisition parameters as used in the T_1 sequence for the determination of the *in vitro* calibration curve. The pulse width of the 90° sinc excitation pulse was optimized for a slice thickness of 4 mm. Eight TIs were used between 0.8 and 8 s, TR = 12 s, NS = 4, total measurement time 384 s. Two T_1 measurements were performed before carbogen breathing and subsequently two during carbogen breathing.

To obtain an *in vivo* $1/T_1$ value for the calibration curve at pO_2 = 0 mmHg, four independent *in vivo* experiments in mice were performed. T_1-values of ^{19}F-spins before and every 6 min after the killing of mice were determined with the slice-selective inversion-recovery T_1 sequence, as described earlier. Mice were killed by switching off the oxygen supply and, 1 min afterward, the total supply of anesthesia was stopped. Experiments on dead mice were finished when T_1 values of ^{19}F-spins reached a steady state. The temperature of the skin adjacent to tumor tissue was monitored on line and was kept at 36°–37° C using the same feedback system and rectal probe as mentioned above. Note that the T_1-relaxation time of ^{19}F-spins is not only related to the oxygen tension in tissue, but also to tissue temperature. Therefore, temperature control is important in all experiments.

Data analysis. From 3 independent *in vitro* measurements, the calibration curve, $1/T_1$ (s^{-1}) vs. pO_2 (mmHg), was obtained by linear regression analysis with Graphpad software (Graphpad PRISM, version 2.0, San Diego, CA). As the intercept value of the calibration curve at pO_2 = 0 mmHg, the mean $1/T_1$ as measured in 4 dead mice was applied. This calibration curve was used to convert *in vivo* T_1 relaxation rates (R_1) of ^{19}F-spins to $pO_{2/relaxo}$ values. The standard errors of the intercept value and the slope of the calibration curve were propagated in the calculations of the SEM of absolute mean $pO_{2/relaxo}$ values per tumor slice in experiments without carbogen breathing (n = 2) or were propagated in calculations of the SE of changes in the $pO_{2/relaxo}$ values after 8 and 14 min carbogen breathing. For carbogen breathing experiments, the average $pO_{2/relaxo}$ changes of all tumors (n = 13) was analyzed with a paired t test.

Polarographic measurements of the oxygen tension in tumor tissue

One day after the ^{19}F-MR experiments, invasive pO_2 measurements were performed with a computerized polarographic system (KIMOC 6650, Eppendorf, Hamburg). The details of this technique have been described previously (8, 24). Briefly, the intratumoral pO_2 was registered with a polarographic needle ($pO_{2electode}$) with a diameter of 300 μm. The sensitive membrane-covered cathode has a diameter of 17 μm, resulting in a hemispherical measuring volume with a diameter of approximately 50 μm around the tip of the electrode (25).

To reduce the resistance of the skin during the insertion of O_2-electrodes in tumors, a small hole was made in the skin adjacent to tumor tissue using a needle with a similar diameter as the O_2 electrodes. Tissue compression artifacts were minimized with forward movements of the O_2 electrode (500 μm), immediately followed by a backward step of 200 μm (26). Tumor oxygenation measurements were performed along two perpendicular tracks in the comparable tumor slices as used in the slice selective ^{19}F-MR relaxometry. Per track, 12 individual $pO_{2/electrode}$ data points were measured. The drift was < 0.4 %. min^{-1}. $PO_{2/electrode}$ values of a track were omitted, when the tumor started bleeding after insertion of the O_2 electrode. The raw data of the $pO_{2/electrode}$ measurements were exported from the KIMOC device into a personal computer for statistical analysis.

Data analysis. Per tumor slice the median $pO_{2/electrode}$ value of both tracks was calculated (n = 24). Next, in the same slice, the mean of the $pO_{2/electrode}$values was calculated from these sample points that coincided with the PFC distribution in the perfused tumor rim (n = 2). These values appeared to be the first and maximum values of the sampled data points in both tracks; therefore, this physiological parameter was denoted as the mean maximum $pO_{2/electrode}$ value. Both the median $pO_{2/electrode}$ value and the mean

maximum $pO_{2/electrode}$ were compared to the absolute mean $pO_{2/relaxo}$ values.

Fluorescence microscopy and (immuno)histochemical analysis of the 2D distribution of perfused microvessels, hypoxic-/necrotic areas, and macrophages

In complete transverse tumor sections, morphometric analysis of perfused microvessels, hypoxic-/necrotic areas and macrophages were performed using a computer-controlled digital-image analysis system connected to a (fluorescence) microscope. One day after the polarographic measurements, 0.3 ml of a suspension was injected i.p. that contained the following chemical compounds: 0.5 ml dimethylsulphoxide, 4.5 ml heated peanut oil, and 70 mg of the hypoxia marker 7(-)[4′-(2-nitroimidazol-l-yl)-butyl]-theophylline (NITP, a generous gift of Dr. R. Hodgkiss, CRC Gray Laboratory, Mount Vernon Hospital, Northwood, Middlesex, UK). Two hours after administration of the hypoxic marker NITP, a 0.05-ml solution of saline (0.9%, pH = 7.4) containing a fluorescent perfusion marker Hoechst 33342 (15 mg/kg, Sigma, St. Louis, MO) was injected i.v. *via* a lateral tail vein. One minute after Hoechst injection, mice were rapidly killed by dislocation of their necks, and tumors were quickly removed and frozen in liquid nitrogen, preventing the redistribution of fluorescent perfusion marker Hoechst. Tumors were cut in half: one half was used for quantitative immunohistochemical analysis of perfused microvessels, the total microvascular bed, hypoxic areas, and the 2D distribution of macrophages. The other half was used for classical histological staining with eosin (cytoplasm) and hematoxylin (nuclei). For each tumor half, three frozen tissue sections (5 μm) at comparable locations as the slices in ^{19}F-MR relaxometry experiments were made. The staining with eosin and hematoxylin was used to distinguish viable tumor areas from necrotic areas.

Immunohistochemical analysis. The different cells and cell structures were analyzed in four steps: the perfused microvessels were analyzed first, followed by the immunohistochemical staining of hypoxic areas, the endothelium of all microvessels, and macrophages. After each staining step, sections were scanned using an extended version of the digital image analysis system as described by Rijken *et al.* (19). After processing all fields of each scan, a composite image was reconstructed from the individual processed fields, revealing the different structures. If the composite images of the tumor sections obtained after each step were combined, then the new matched image showed the 2D distribution of perfused microvessels, hypoxic areas, the total microvascular bed, and macrophages.

For the staining of hypoxic areas, sections were incubated with rabbit antitheophylline (Sigma, St. Louis, MO), followed by incubation with FITC-labeled donkey antirabbit immunoglobulin (Jackson ImmunoResearch Laboratories, West Grove, PA). The endothelium of all microvessels was first stained with monoclonal rat antimouse antibody ME 9F1 (27), followed by the second and third antibody TRITC-labeled goat antirat immunoglobulin and donkey antigoat immunoglobulin (Jackson ImmunoResearch Laboratories). In different tumor sections, but adjacent to sections with hypoxic cell staining, the macrophages were stained with monoclonal rat antibody to mouse macrophage (clone F4/80, rat IgG-2b, Caltag laboratories, Burlingame, CA). The second antibody was rhodamine-labeled rabbit antirat IgG (Cappel-Organon Technika, Durham, NC). In the same sections as used for the analysis of the macrophage distribution, the basal lamina of the tumor vasculature was stained with collagen Type IV poly-clonal antibody (goat antitype IV collagen, Southern Biotechnology Associates, Birmingham, AL) and donkey antigoat immunoglobulin labeled with FITC (Jackson ImmunoResearch Laboratories).

Data analysis. Per tumor section, the 2D distribution of macrophages, perfused microvessels, hypoxic, and necrotic areas was compared to the 2D distribution of PFC compounds in ^{19}F-SE density MR images and the 2D distribution of high-intensity regions in T_2-weighted ^{1}H-SE MR images, respectively. Per tumor section, the hypoxic fraction and the necrotic fraction were calculated. Both parameters are defined as the total hypoxic or necrotic area per total tumor section area. Next, an average necrotic and hypoxic fraction was calculated for all tumors (n = 13).

RESULTS

Calibration curve for oxygen tension measurements by ^{19}F-MR relaxometry

In vitro ^{19}F-MR relaxometry measurements of the PFC emulsion (40%, v/v) at a temperature of 37° C for 5 different oxygen tensions (pO_2, mmHg) resulted in the following calibration curve:

$$\frac{1}{T_1} = 0.44 + 0.0028.pO_2$$

The standard error (SE) of the intercept value [0.44 (s^{-1})] is 2.3%, and the SE of the slope [0.0028 (s.mmHg)$^{-1}$] is 1%. The $1/T_1$ value obtained from the *in vivo* ^{19}F-MR relaxometry studies on 4 dead mice was: 0.41 ± 0.02 (SEM) s^{-1}. This $1/T_1$ value is not significantly different from the intercept value of the *in vitro* measurements. For calculations of absolute mean $pO_{2/relaxo}$ values in the following sections, this value of 0.41 s^{-1} was used as intercept. It should be noted that the intercept is not needed for calculations of changes in the $pO_{2/relaxo}$ values.

Comparison of the 2D distribution of PFCs in ^{19}F-SE density MR images and high-intensity areas in T_2-weighted ^{1}H-SE MR images with the 2D distribution of perfused microvessels, hypoxic -/necrotic areas, and macrophages

Three days after i.v. injection of PFCs, the 2D distribution of PFCs in ^{19}F-SE density images corresponds mainly to the 2D distribution of perfused microvessels in Hoechst images; see, for example, tumors No. 10 and 11 in Fig. 1A

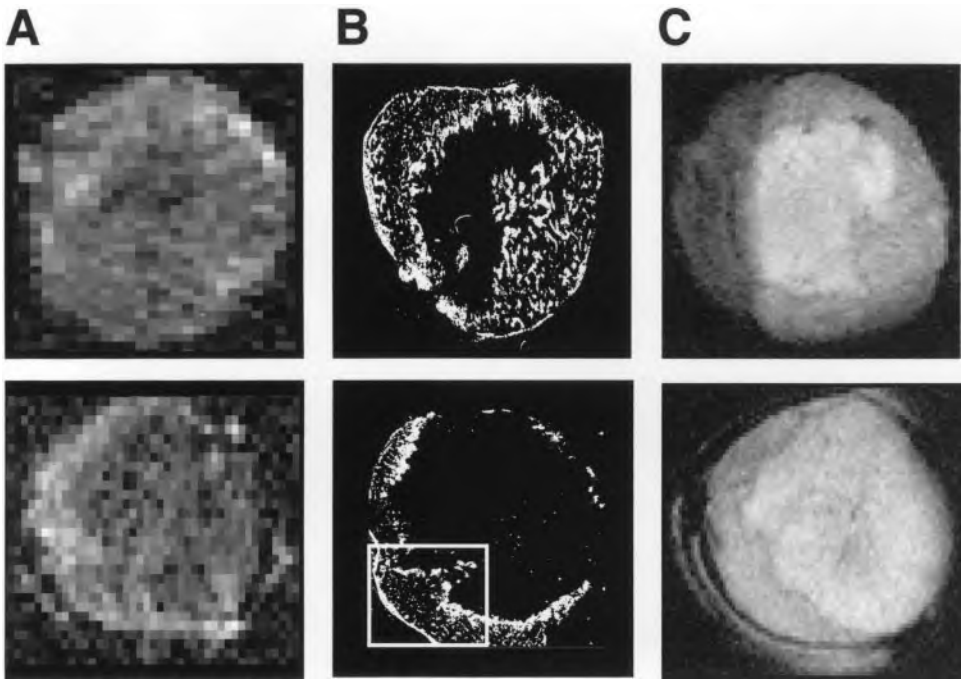

Fig. 1. (A) The PFC distribution in ^{19}F-SE density MR-images of a slice through the center of tumors No. 10 and No. 11. (B) The 2D perfused microvessel (white structures) distribution in fluorescence microscopic Hoechst images of comparable slices. (C) The ^{1}H-signal intensities in T_2-weighted ^{1}H-SE MR-images in similar slices as the ^{19}F-MRI studies. Detailed analyses of the delineated area in (B) are given in Fig. 2.

and 1B. All tumors were well perfused in the periphery and no perfused microvessels were detected in the center. The nonperfused regions in Hoechst images correlated with high intensity areas in T_2-weighted ^{1}H-SE MR images (Fig. 1B and C). A detailed analysis of such a nonperfused area is shown in Fig. 2 for tumor No. 10. In eosin- and hematoxylin-stained sections, these areas appeared necrotic (Fig. 2B). The average necrotic fraction of all 13 tumors was 0.5 ± 0.06 (SEM) (-). In only 5 of the 13 tumors, NITP-labeled cells (~ hypoxic cells) could be detected. The average hypoxic fraction of these 5 tumors was 0.01 ± 0.0013 (SEM) (-). In general, a thin layer of NITP-labeled cells surrounded extensive necrotic cords; see, for example, tumor No. 2 in Fig. 3A and 3B. For this tumor line, comparable results were obtained with another hypoxic marker, pimonidazole hydrochloride (PIMO) (P. Rijken M.Sc., oral communication, November 1997). In only one tumor, a small isolated group of macrophages was observed in the perfused tumor rim (results not shown), of which the 2D distribution did not correlate with the distribution of PFCs.

Comparison of median $pO_{2/electrode}$ values with absolute mean $pO_{2/relaxo}$values in tumor tissue slices

Low S:N ratios in ^{19}F-MR spectra of PFCs in the whole tumor did not permit voxel-selective T_1 measurements or local $pO_{2/relaxo}$ studies within a reasonable time (11). Absolute mean $pO_{2/relaxo}$ values were measured in perfused regions of the tumor throughout the whole MR slice (see previous paragraph), and ranged from 0.03 to 49.7 mmHg (see Table 1). In tumor No. 4, with a mean $pO_{2/relaxo}$ value of 49.7 mmHg, an important region with low ^{1}H signal intensities was found near the center of the tumor in T_2-weighted ^{1}H-SE MR images, probably corresponding to extravasation of hemoglobin.

In this region, the blood oxygen tension directly effects the T_1 relaxation time of ^{19}F-spins of PFC compounds, which may result in high $pO_{2/relaxo}$ values.

Polarographic measurements were done in two perpendicular tracks located within the slices, as measured in the corresponding *in vivo* ^{19}F-MR relaxometry studies. For tumor No. 10, a fluorescence microscopic image (Hoechst image) of the perfused microvessel distribution is displayed in Fig. 4A, including the approximate locations of the tracks. The $pO_{2/electrode}$ values obtained during the stepwise movement of the Eppendorf electrode in one track are shown in Fig. 4B. The $pO_{2/electrode}$ values decreased from the periphery of the tumor to the center. Median $pO_{2/electrode}$ values of tumors denoted by asterisks in Table 1 varied from 0.4 to 3.3 mmHg. Four of the 13 tumors started bleeding during the insertion of O_2 electrodes and data were not further evaluated. Tissue injuries related to the Eppendorf electrode measurements were only observed in 2 of 9 remaining tumors, but this did not influence the (immuno) histochemical analysis in whole tumor sections because $pO_{2/electrode}$ values were locally sampled in two tracks.

For the tumors studied by both methods, the median $pO_{2/electrode}$ values were generally lower than the mean $pO_{2/relaxo}$ values (Fig. 5). However, when the mean *maximum* $pO_{2/electrode}$ values that originated from the tumor

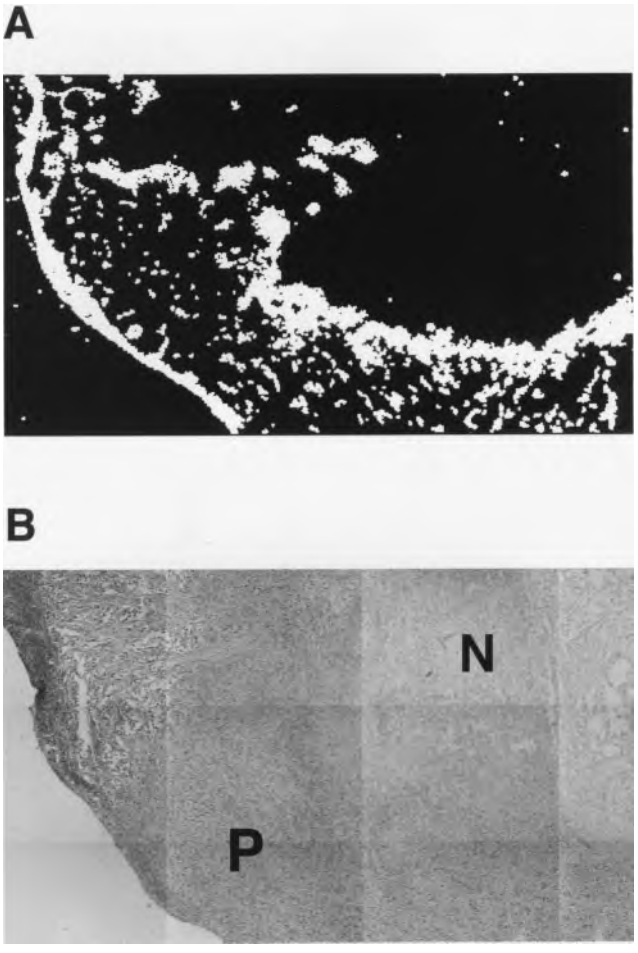

Fig. 2. Representative results of histological analysis of nonperfused regions in tumor No. 10 are shown here. An area of Fig. 1B delineated by the rectangle is analyzed in more detail in (A) and (B). (A) shows the distribution of perfused microvessels (white structures) and, in (B), the results of the haematoxylin (nuclei) and eosin (cytoplasm) staining (HE) are displayed. The light grey colors correspond to necrotic areas (N) and the darker grey colors are related to perfused tumor areas (P) in (A).

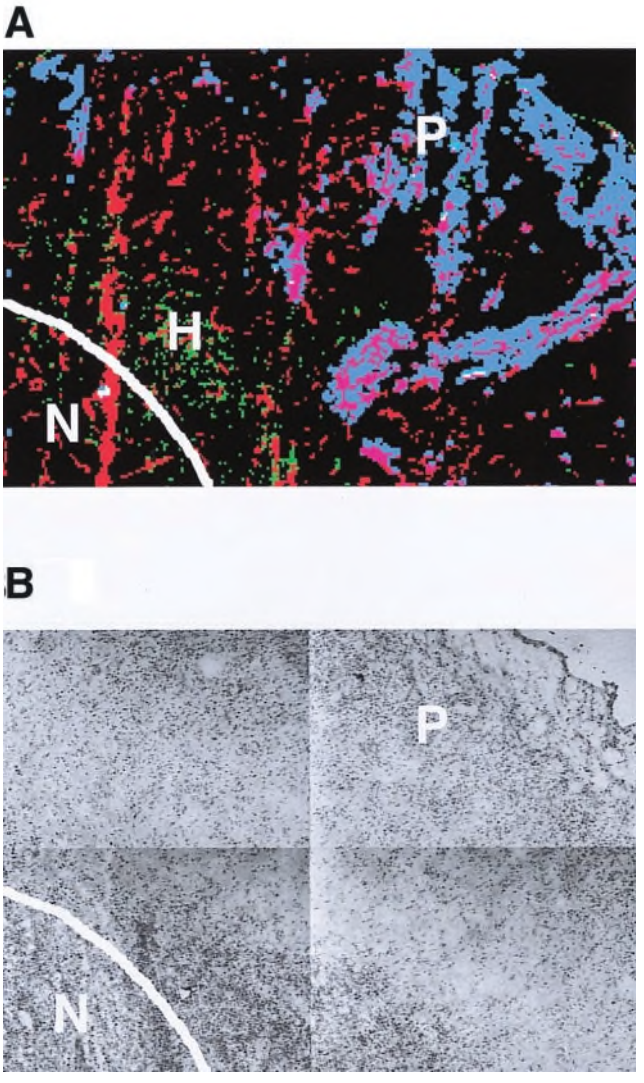

Fig. 3. A detailed analysis of hypoxic and necrotic areas of tumor No. 2 is depicted in (A) and (B), respectively. Three different (cell) structures were labeled in (A): perfused microvessels (P, blue), endothelium of all microvessels (red), and hypoxic cells (H, green). Hypoxic cells appear at a distance of 100–150 μm from perfused microvessels. Differences between the staining of nuclei (hematoxylin) and cytoplasm (eosin) in necrotic regions and areas with viable tissue are shown in (B). The perfused and viable tissue regions (P) have a more uniform nuclei staining than necrotic regions (N).

periphery were compared with mean $pO_{2/relaxo}$ values, a much closer correlation between both data sets was observed, as indicated by the solid line in Fig. 5 (= approaching the line of identity). Finally, no relationships were found between necrotic and hypoxic fractions and mean $pO_{2/relaxo}$ values or median $pO_{2/electrode}$ values.

In vivo ^{19}F-MR relaxometry studies of the oxygen tension changes in tumor tissue during carbogen breathing

Changes in the $pO_{2/relaxo}$ values were measured in complete tumor tissue slices. Table 1 presents the $pO_{2/relaxo}$ changes in slices through the center of 13 tumors after 8 and 14 min of carbogen breathing.

After 8-min carbogen breathing, a small increase of the $pO_{2/relaxo}$ tensions relative to baseline was observed in 12 of the 13 mice. The $pO_{2/relaxo}$ changes were rather heterogeneous and varied from 0.03 to 15 mmHg. The average oxygen tension increase ($\Delta pO_{2/relaxo}$) of all tumors (except tumor No. 4) = 3.3 ± 0.8 (SEM) mmHg and was significantly different from zero ($p < 0.01$).

In 9 of 13 mice, the increase of the $pO_{2/relaxo}$ values reduced after 14-min carbogen breathing: these values relative to baseline varied from 0.1 to 6.6 mmHg. The average $\Delta pO_{2/relaxo}$ was 2.1 ± 0.6 (SEM) mmHg, which still was significantly different from zero ($p < 0.05$), but was not significantly different from changes after 8-min carbogen breathing ($p > 0.05$).

DISCUSSION

In contrast to polarographic measurements, ^{19}F-MR relaxometry of perfluorocarbon compounds permits noninva-

Table 1. *In vivo* ^{19}F-MR relaxometry measurements of absolute mean $pO_{2/relaxo}$ values (mmHg) and changes in $pO_{2/relaxo}$ values relative to baseline ($\Delta pO_{2/relaxo}$, mmHg) after 8- and 14-min carbogen breathing

No.	Volume (cm^3)	$mpO_{2/relaxo}$	$\Delta pO_{2/relaxo}$ (8 min)	$\Delta pO_{2/relaxo}$ (14 min)
1*	0.70	8.8 ± 0.6	2.8 ± 4.3	0.2 ± 3.0
2*	1.10	0.3 ± 1.0	2.3 ± 3.4	0.7 ± 3.7
3*	0.60	8.6 ± 0.6	4.1 ± 5.1	0.9 ± 4.1
4	0.41	49.7 ± 2.5	15.1 ± 11	1.7 ± 7.2
5*	0.56	0.8 ± 0.4	2.7 ± 4.3	3.5 ± 5.0
6*	0.65	2.8 ± 0.9	0.5 ± 3.5	2.1 ± 4.0
7*	0.30	0.03 ± 3.0	5.3 ± 3.7	1.2 ± 3.5
8	0.31	9.1 ± 0.2	9.3 ± 5.8	6.6 ± 3.1
9	0.40	8.4 ± 0.1	5.0 ± 4.0	5.4 ± 3.6
10*	0.41	8.7 ± 0.9	2.8 ± 3.4	0.4 ± 3.7
11*	0.34	0.9 ± 0.4	0.03 ± 3.7	1.3 ± 3.5
12	0.37	13.5 ± 1.4	5.9 ± 3.6	0.1 ± 3.6
13*	0.39	3.1 ± 0.5	0.6 ± 4.9	3.5 ± 5.6

In tumors denoted by an asterisk, the oxygen tension was also measured by polarography (Fig. 5). The values in column 3 are means ± SEM. The values in column 4 and 5 are mentioned with their SE.

sive oxygen tension measurements, independent of the location of the tumor. However, this new method does not allow direct analysis of the oxygen tension: local oxygen tensions are derived from T_1 relaxation rates of ^{19}F-spins in the perfluorocarbon compounds. These relaxation rates may also depend on other physiological and histological parameters and, therefore, $pO_{2/relaxo}$ values have been compared to $pO_{2/electrode}$ values in this study. In addition to ^{19}F-MR relaxometry and polarographic studies, the spatial distribution of PFC compounds over the tumor was determined and correlated to the location of the oxygen electrodes in tumor tissue, and to the distribution of perfused microvessels, hypoxic, and necrotic areas. In this way, a proper comparison between both techniques becomes possible, because the tumor areas from which the measured $pO_{2/relaxo}$ and $pO_{2/electrode}$ values originate are known.

Calibration curve

The relationship between the T_1 relaxation rates ($1/T_1$) of ^{19}F-spins in perfluoro-15-crown-5-ether and oxygen tensions was determined under strict temperature control, because T_1 relaxation rates of PFCs also have an inverse relationship with temperature (11). The intercept and slope value of the calibration curve of the neat perfluoro-15-crown-5-ether obtained in this study were larger than the values reported elsewhere (11). This may be due to a number of differences in experimental conditions, such as the ways to control temperature and to maintain O_2 levels during the *in vitro* ^{19}F-MR relaxometry examinations. In the present study, the intercept values obtained from *in vitro* studies and ^{19}F-MR experiments on dead mice were not significantly different using the same temperature control system. These results indicate that the temperature of the tumors and the emulsion was comparable and differences in physiological properties, such as salt concentrations, pH, presence of proteins, and PFC concentrations do not influence the T_1 relaxation rates of PFCs (16, 28). A simultaneous determination of tissue temperature and tissue oxygen tensions would be necessary to exclude the effect of temperature differences on T_1 relaxation rates of PFCs. This is possible with PFCs, which have two or more resonances in ^{19}F-MR spectra (14), but this cannot be done with perfluoro-15-crown-5-ether, which has 20 equivalent fluorine atoms resonating at a single frequency. The correlation between the $pO_{2/relaxo}$ and $pO_{2/electrode}$ data in this study suggest that the calibration curve is reliable and can be used to convert in vivo $1/T_1$ values of ^{19}F-spins of PFCs to *in vivo* $pO_{2/relaxo}$ values.

In vivo ^{19}F-MR relaxometry studies and polarographic measurements of oxygen tensions in tissue slices of human glioma xenografts

Dardzinski and Sotak (11) used a fast MR imaging technique to measure voxel-selective T_1 relaxation rates of perfluoro-15-crown-5-ether or local oxygen tensions. In the present study, low signal-to–noise ratios in ^{19}F-MR spectra of PFCs in the whole tumor did not permit performance of such studies within a reasonable time. The signal-to–noise ratios were lower, because the amount of administrated perfluoro-15-crown-5-ether had to be 2.4 times smaller than the dose used in the studies reported by Dardzinski and Sotak (11). Their dose was lethal to nude mice in our study. In addition, the permeability of microvessels for perfluoro-15-crown-5-ether in RIF-1 tumors may be larger than the permeability of microvessels in the glioma xenograft line used in the present study. Intertumoral variations of microvessel permeability for perfluoro-15-crown-5-ether were also observed in different glioma xenograft lines (results not shown).

Three days after i.v. administration, the perfluorocarbons became mainly sequestered in the well-perfused rim of the human glioma xenografts, as observed in ^{19}F-SE density MR images and histological analysis. In a previous study, these histological analyses of the 2D perfused vascular

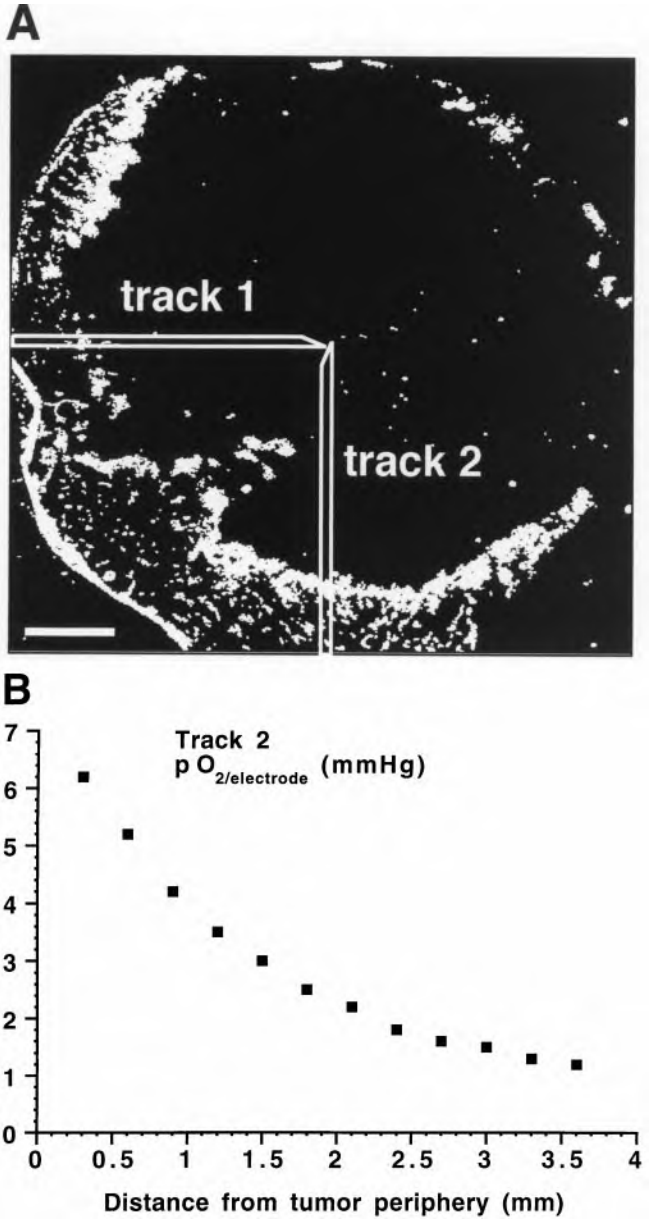

Fig. 4. A fluorescence microscopic image (Hoechst image) of the 2D distribution of perfused microvessels (white structures) in a slice through the center of tumor No. 10 is shown in (A).The length of the white bar corresponds to 1 mm. Also in (A), the approximate locations of two perpendicular tracks of the O_2-electrode are displayed. (B) The individual $pO_{2/electrode}$ values (mmHg) of track No. 2 (*y* axis) as obtained during the stepwise movement of the Eppendorf electrode from the periphery of the tumor to the center (*x* axis) (stepsize 0.3 mm, total length of track 3.6 mm).

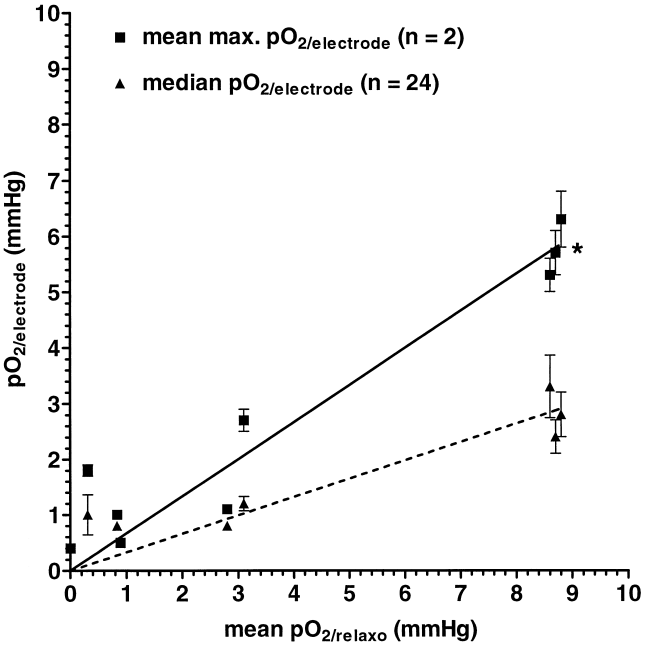

Fig. 5. Comparison between absolute mean $pO_{2/relaxo}$ values (mmHg) per tumor tissue slice and median $pO_{2/electrode}$ values ± SEM (dashed line) or mean *maximum* $pO_{2/electrode}$ values ± SEM (solid line) as detected in 2 perpendicular tracks in comparable slices (Fig. 4). The lines indicate the results of least squares linear regression analysis ($R^2 = 0.96$, solid line and $R^2 = 0.95$, dashed line) using Graphpad PRISM software (version 2.0, San Diego, CA). Both lines were forced to go through the origin during the regression analysis. Detailed analyses of tumor No. 10 denoted by an asterisk (*) are given in Fig. 4.

architecture have been validated by fast dynamic ^{1}H-MR imaging studies of contrast-agent uptake (29). One minute after bolus injection, the 2D distribution of the contrast agent in ^{1}H-MR images was found to be similar to the distribution of perfused microvessels 1 min after the injection of the fluorescent marker Hoechst. In the present study, the PFC distribution did not spatially correlate with the distribution of macrophages; thus, these cells, as suggested by Longmaid *et al.* (18), do not take up PFCs. The long-term retention of PFCs in perfused regions indicates, however, that they are firmly bound to tissue or cell structures in perfused regions of the tumor, rather than redistributed in the whole tumor volume. The latter hypothesis could not be tested with (immuno) histochemical methods applied in the present paper because analysis at the subcellular level were not possible. Mason *et al.* (15) suggested also that PFCs became sequestered in well-perfused regions of Dunning prostate tumors, but did not provide any evidence for this suggestion. In this study, and probably in the study of Mason *et al.* (15), absolute mean $pO_{2/relaxo}$ values and changes in $pO_{2/relaxo}$ tensions are mainly measured in perfused regions of tumors.

However, in the evaluation phase before radiotherapy, oxygen tension measurements in chronically hypoxic areas appear of greater interest than pO_2 measurements in perfused regions of tumors. In immunohistochemical analysis of chronically hypoxic cells with the bioreductive chemical probe NITP, a thin layer of NITP-labeled cells was found adjacent to extensive necrotic cords in a few human glioma xenografts. In some tumors, hypoxic cells as detected by NITP were even absent. In general, hypoxic areas were much smaller than perfused tumor regions that contain most of the PFCs. Therefore, oxygen tension measurements in hypoxic areas using ^{19}F-MR relaxometry seems not possible

in the tumor line used in the present study. Other human glioma xenograft lines showed larger areas with NITP-labeled cells (Paul Rijken M.Sc., oral communication, November 1998). In these tumor models, intratumoral injections of PFCs is an attractive alternative i.v. administration of PFCs to assess tissue pO_2 in hypoxic regions (15, 17). However, also in this approach, hypoxic areas may not be included because these cannot be selected beforehand.

In the well-perfused tumor rim, the mean oxygen tensions as measured by ^{19}F-MR-relaxometry ($pO_{2/relaxo}$) were comparable to the mean of the maximum $pO_{2/electrode}$ values of both tracks that originate from the same perfused tumor rim. The absolute mean oxygen tension values in perfused regions were found to be relatively low in both analyses. Others also obtained low oxygen tension values in animal tumor models using polarographic or ^{19}F-MR relaxometry measurements (8, 13, 17, 30–34). Recent phosphorescence quenching microscopic analysis of pO_2 profiles in human colon adenocarcinoma xenografts with a spatial resolution of 10 μm showed that the pO_2 near perfused microvessels was approximately 14 mmHg and decreases monotonically until hypoxic values ($<$ 5 mmHg) at a distance of 70–80 μm away from the nearest capillary wall (35). The mean pO_2 along the distance of 80 μm was approximately 8.4 mmHg, which is comparable to maximum $pO_{2/relaxo}$ and $pO_{2/electrode}$ values as measured in the perfused rim of the glioma xenograft line in this study. Although O_2 consumption rates of tumor cells and O_2 diffusion coefficient may not be similar in human glioma xenografts, these results suggest that slice-selective ^{19}F-MR relaxometry measurements of PFCs sequestered in the perfused rim of tumors probe a mean oxygen tension of O_2 profiles pertinent to perfused microvessels. The same is probably true for polarographic analysis of oxygen tensions, because the sample area of the O_2 electrode has approximately a diameter of 50 μm (25). Therefore, the mean maximum $pO_{2/electrode}$ values in the perfused tumor rim were comparable to mean $pO_{2/relaxo}$ values. If the median $pO_{2/electrode}$ value of both tracks was calculated, then this value was lower than the mean $pO_{2/relaxo}$ value because low $pO_{2/electrode}$ values that originated from hypoxic and necrotic areas were also included in calculations of the median $pO_{2/electrode}$ values.

Effect of carbogen breathing on the mean $pO_{2/relaxo}$ values in tumor tissue slices

In this study, ^{19}F-MR relaxometry measurements of i.v. injected PFCs did not only permit the determination of oxygen tensions in perfused areas, but also oxygen tension changes. A small but significant increase of the $pO_{2/relaxo}$ values was observed after 8- and 14-min carbogen breathing. In 9 of the 13 mice, this increase tended to become smaller after 14-min carbogen breathing. If oxygen tension changes in perfused areas may cause radiosensitization, then maximum radiosensitivity is expected within the first 8 min after the start of carbogen breathing. ^{19}F-MR relaxometry measurements alone cannot give an explanation for this small decrease of $pO_{2/relaxo}$ values during carbogen breathing, but we may speculate that this has to do with the redistribution of O_2 by diffusion in tumor tissue after the start of carbogen breathing and/or the time to establish a new equilibrium between the increased O_2 supply and demand.

In the context of radiotherapy, the detection of oxygen tension changes in chronically hypoxic areas are of greater interest. Perhaps the use of fluorinated bioreductive chemical probes may assess oxygen tension changes in chronically hypoxic regions noninvasively by ^{19}F-MR spectroscopy, although MR sensitivity may limit their proper detection (36–39).

CONCLUSIONS

If perfluorocarbon compounds are administrated 3 days before the slice-selective ^{19}F-MR relaxometry experiments, then oxygen tensions and oxygen tension changes during carbogen breathing are mainly measured in perfused regions of the tumor throughout the whole MR slice. In these regions, mean $pO_{2/relaxo}$ tensions have been validated by polarographic measurements. The effect of carbogen breathing on the oxygen tension in perfused areas was small, but significant, and tended to decrease with time.

REFERENCES

1. Denekamp J. Does physiological hypoxia matter in cancer therapy? In: Steel GG, Adams GE, Peckham MJ, editors. The biological basis of radiotherapy. Amsterdam, NY, Oxford: Elsevier; 1983. p. 139–155.
2. Gray LH, Conger AD, Ebert M, *et al*. The concentration of oxygen dissolved in tissues at the time of irradiation as a factor in radiotherapy. *Br J Radiol* 1953;26:638–648.
3. Moulder JE, Rockwell S. Hypoxic fractions of solid tumors, experimental technique, methods of analysis and a survey of existing data. *Int J Radiat Oncol Biol Phys* 1984;10:695–712.
4. Chaplin DJ, Horsman MR, Siemann DW. Further evaluation of nicotinamide and carbogen as a strategy to reoxygenate hypoxic cells in vivo: Importance of nicotinamide dose and preirradiation breathing time. *Br J Cancer* 1993;68:269–273.
5. Rojas A, Joiner MC, Hodgkiss RJ, *et al*. Enhancement of tumor radiosensitivity and reduced hypoxia-dependent binding of a 2 nitroimidazole with normobaric oxygen and carbogen: A therapeutic comparison with skin and kidneys. *Int J Radiat Oncol Biol Phys* 1992;23:361–366.
6. Siemann DW, Hill RP, Bush RS. The importance of the preirradiation breathing times of oxygen and carbogen (5% CO_2: 95% O_2) on the in vivo radiation response of a murine sarcoma. *Int J Radiat Oncol Biol Phys* 1977;2:903–911.
7. Kaanders JHAM, Pop LAM, Marres HAM, *et al.* Accelerated radiotherapy with carbogen and nicotinamide (ARCON) for laryngeal cancer. *Radiother Oncol* 1998;48:115–122.
8. Kallinowski F, Zander R, Hoeckel M, *et al*. Tumor tissue oxygenation as evaluated by computerized-pO_2-histography. *Int J Radiat Oncol Biol Phys* 1990;19:953–961.
9. Vaupel P, Schlenger K, Knoop C, *et al*. Oxygenation of human tumors: Evaluation of tissue oxygen distribution in

breast cancers by computerized O_2 tension measurements. *Cancer Res* 1991;51:3316–3322.
10. Baldwin NJ, Ng TC. Oxygenation and metabolic status of KHT tumors as measured simultaneously by ^{19}F magnetic resonance imaging and ^{31}P magnetic resonance spectroscopy. *Magn Reson Imaging* 1996;14(5):541–551.
11. Dardzinski BJ, Sotak CH. Rapid tissue oxygen tension mapping using ^{19}F inversion-recovery echo-planar imaging of perfluoro-15-crown-5-ether. *Magn Reson Med* 1994;32:88–97.
12. Hees PS, Sotak CH. Assessment of changes in murine tumor oxygenation in response to nicotinamide using ^{19}F NMR relaxometry of a perfluorocarbon emulsion. *Magn Reson Med* 1993;29:303–310.
13. Mason RP, Nunnally RL, Antich PP. Tissue oxygenation: A novel determination using ^{19}F surface coil nmr spectroscopy of sequestered perfluorocarbon compounds. *Magn Reson Med* 1991;18:71–79.
14. Mason RP, Shukla H, Antich PP. In vivo oxygen tension and temperature: simultaneous determination using ^{19}F NMR spectroscopy of perfluorocarbon. *Magn Reson Med* 1994;29: 296–302.
15. Mason RP, Antich PP, Babcock EE, *et al*. Non-invasive determination of tumor oxygen tension and local variation with growth. *Int J Radiat Oncol Biol Phys* 1994;29(1):95–103.
16. Mason RP. Non-invasive physiology: ^{19}F NMR of perfluorocarbons. *Art Cells Blood Subs Immob Biotech* 1994;22(4): 1141–1153.
17. Mason RP, Rodbumrung W, Antich PP. Hexafluorobenzene: a sensitive ^{19}F NMR indicator of tumor oxygenation. *NMR Biomed* 1996;9:125–134.
18. Longmaid HE, Adams DF, Neirinckx RD, *et al*. R.P. *In vivo* ^{19}F imaging of liver, tumor, and abscess in rats: preliminary results. *Invest Radiol* 1985;20:141–145.
19. Rijken PFJW, Bernsen HJJA, van der Kogel AJ. Application of an image analysis system to the quantitation of tumor perfusion and vascularity in human glioma xenografts. *Microvascular Res* 1995;50:141–153.
20. Bernsen HJJA, Rijken PFJW, Oostendorp T, *et al*. Vascularity and perfusion of human gliomas xenografted in the athymic nude mouse. *Br J Cancer* 1995;71(4):721–726.
21. van der Sanden BPJ, Heerschap A, van der Toorn A, *et al*. Effect of carbogen breathing on the physiological profile of human glioma xenografts. *Magn Res Med* 1999; in press.
22. Silver MS, Joseph RI, Hoult DI. Highly selective $\pi/2$ and π pulse generation. *J Magn Reson* 1984;59:347–351.
23. Maier CF, Paran Y, Bendel P, *et al*. Quantitative diffusion imaging in implanted human breast tumors. *Magn Reson Med* 1997;37:576–581.
24. Stüben G, Stuschke M, Kühmann K, *et al*. The effect of combined nicotinamide and carbogen treatments in human tumour xenografts: oxygenation and tumor control studies. *Radiother Oncol* 1999; in press.
25. Vaupel PW, Kelleher DK. Tumor oxygenation. In: Vaupel PW, Kelleher DK, Gunderoth M, editors. Functionsanalyse biologischer Systeme 24. Stuttgart: Gustav Fischer Verlag; 1995. p. 336.
26. Vaupel P, Kallinowski F, Okunieff P. Blood flow, oxygen and nutrient supply and metabolic microenvironment of human tumors: a review. *Cancer Res* 1989;49:6449–6465.
27. Westphal JR, van 't Hullenaar RGM, van der Laak JAWM, *et al*. Vascular density in melanoma xenografts correlates with vascular permeability factor expression but not with metastatic potential. *Br J Cancer* 1997;76(5):561–570.
28. Thomas SR, Pratt RG, Millard RW, *et al*. Evaluation of the influence of the aqueous phase bioconstituent environment on the F-19 T1 of perfluorocarbon blood substitute emulsions. *JMRI* 1994;4:631–635.
29. van der Sanden BPJ, de Graaf RA, Rijken PFJW, *et al*. A comparative study of dynamic ^{1}H-MRI studies of Gd−DTPA uptake, perfused vessel distribution and hypoxic areas in human glioma xenografts. (Abstr.) Proceedings of the 5th ISMRM meeting,Vancouver 1997. p. 1087.
30. Goda F, O'Hara JA, Rhodes ES, *et al*. Changes of oxygen tension in experimental tumors after a single dose of X-ray irradiation. *Cancer Res* 1995;55:2249–2252.
31. Kelleher DK, Vaupel P. The effect of nicotinamide on microcirculatory function, tissue oxygenation and bioenergetic status in rat tumors. (Abstr.) In : Vaupel P, editors. Oxygen transport to tissue XV. New York: Plenum Press; 1994. p. 395–402.
32. Lee I, Boucher Y, Demhartner TJ, *et al*. Changes in tumour blood flow, oxygenation and interstitial fluid pressure induced by pentoxifylline. *Br J Cancer* 1994;69:492–496.
33. Nozue M, Lee I, Hartford A, *et al*. pO_2 measurements in murine tumors by Eppendorf 'Histograph' : Calibration, reproducibility and comparison with diamond-general device. *Int J Oncol* 1996;9:995–962.
34. Thomas CD, Chavaudra N, Martin L, *et al*. Correlation between radiosensitivity, percentage hypoxic cells and pO_2 measurements in one rodent and two human tumor xenografts. *Radiat Res* 1994;139:1–8.
35. Helmlinger G, Yuan F, Dellian M, *et al*. Interstitial pH and pO_2 gradients in solid tumors in vivo: High-resolution measurements reveal a lack of correlation. *Nature Med* 1997;3(2): 177–182.
36. Aboagye EO, Maxwell RJ, Kelson AB, *et al*. Preclinical evaluation of the fluorinated 2-nitroimidazole N-(2-hydroxy-3,3,3-trifluoropropyl)-2-(2-nitro-1-imidazolyl) acetamide (SR-4554) as a probe for the measurement of tumor hypoxia. *Cancer Res* 1997;57:3314–3318.
37. Kwock L, Gill M, McMurry HL, *et al*. Evaluation of a fluorinated 2-nitroimidazole binding to hypoxic cells in tumor-bearing rats by ^{19}F magnetic resonance spectroscopy and immunohistochemistry. *Radiat Res* 1992;129:71–78.
38. Maxwell RJ, Workman P, Griffiths JR. Demonstration of tumor-selective retention of fluorinated nitroimidazole probes by ^{19}F magnetic resonance spectroscopy *in vivo*. *Int J Radiat Oncol Biol Phys* 1988;16:925–929.
39. Raleigh JA, Franko AJ, Kelly DA, *et al*. Development of an *in- vivo* ^{19}F magnetic resonance method for measuring oxygen deficiency in tumors. *Magn Reson Med* 1991;22:451–466.